ACCELERATORS

Observation of optical transition radiation from electron beams generated by laser plasma accelerator

Observation of optical transition radiation from electron beams generated by laser plasma accelerator

LIN Chen(林晨)[1] K. Nakamura[2] J. Van Tilborg[2] A. J. Gonsalves[2]
T. Sokollik[2,3] S. Shiraishi[2] W. P. Leemans[2] GUO Zhi-Yu(郭之虞)[1]

[1] State Key Laboratory of Nuclear Physics and Technology, Peking University, Beijing 100871, China
[2] Lawrence Berkeley National Laboratory, Berkeley, CA, 94720, USA
[3] University of California, Berkeley, CA, 94720, USA

Abstract: Laser plasma accelerators (LPAs) have made great progress, achieving electron beam with energy up to 1 GeV from a centimeter scale capillary plasma waveguide. Here, we report the measurement of optical transition radiation (OTR) from the capillary-based LPA electron beams. Transition radiation images, produced by electrons passing through two separate foils (located at 2.3 m and 3.8 m away from the exit of the LPA) were recorded with a high resolution imaging system, respectively. Two magnetic quadrupole lenses were placed right after the capillary to focus and collimate the electron beams. Significant localized spikes appeared in the OTR images when the electron beam was focused by the magnetic quadrupole lenses, indicating the coherence of the radiation and the existence of ultrashort longitudinal structures inside the electron beam.

Key words: laser plasma accelerator, optical transition radiation

PACS: 07.77.Ka, 41.60.Dk, 41.75.Jv **DOI:** 10.1088/1674-1137/37/2/027003

1 Introduction

Laser plasma accelerators (LPAs) produce acceleration gradients by the order of tens to hundreds of GV/m, making them attractive as compact particle accelerators [1]. In such accelerators, a focused intense ($>10^{19}$ W/cm^2) laser pulse drives a plasma density wave, oscillating at the plasma wavelength. Electrons with sufficient initial energies are self-trapped and accelerated by the plasma wave to relativistic energies. However, the acceleration length is limited by the order of only a few mm due to the diffraction of the drive laser in the plasma, which is one of the main obstacles for achieving higher electron energies. This limit has been conquered by employing a capillary discharge waveguide, where the laser intensity was effectively maintained over 33 mm interaction length and quasi-monoenergetic electron beams with low divergence and up to 1 GeV energy has been achieved [2]. Simulations and theory indicate that such high energy LPA electron bunches are of sufficiently short duration and high current, to be candidates for drivers of table-top free electron lasers (FELs) [3], which have a broad range of applications. However, the ultrashort beams can experience significant evolution during propagation, due to the initial bunch energy dispersion and emittance, and due to space charge effects. Hence a focusing devise, i.e. quadruple magnet, is necessary to ensure efficient electron-beam transport and the beam quality for the subsequent radiation devises. Implementation of LPA electrons, therefore, requires detailed knowledge of the temporal structure of beams not only at the exit of the accelerator, but also at a working distance which may be tens of centimeters to meters away.

The temporal profile of LPA electron beam has been characterized by coherent transition radiation (CTR) emitted when an electron bunch passes through an interface between two media with different dielectric constants [4]. CTR measured at THz frequencies suggested an upper bound of the bunch duration less than 50 fs [5, 6], as they were resolution limited by the electro-optic crystal properties and probe laser duration. Alternatively, the microstructure inside the electron bunch has been observed using CTR emitted in the far infrared [7] and in the visible range (Coherent OTR) [8], where a fs resolution can be achieved due to the short wavelength of interest. In several FEL facilities, the COTR signal has already been employed to monitor the electron beam microbunching caused by the FEL-related devices [9–12].

The microstructure inside the LPA electron beams [8, 13] is attributed to the direct interaction with the laser. As the beam accelerates and moves forward inside the

Received 19 March 2012

plasma wave, it starts to interact with the drive laser and develops modulated structures on the laser wavelength. The transition radiation energy from an electron beam per unit frequency $\mathrm{d}\omega$ and unit solid angle $\mathrm{d}\Omega$ can be expressed as [14]

$$\frac{\mathrm{d}^2W}{\mathrm{d}\omega\mathrm{d}\Omega}=N|\xi_\mathrm{e}|^2+N(N-1)|F(\omega,\theta)\xi_\mathrm{e}|^2, \qquad (1)$$

where ξ_e is the single electron normalized amplitude of the radiation field, N is the number of electrons in the bunch, θ is the observation angle and the form factor $F(\omega,\theta)=\int\exp(-\mathrm{i}k\cdot r)f(\boldsymbol{r})\mathrm{d}^3r$ is the Fourier transform of the bunch spatial distribution $f(\boldsymbol{r})$. More detailed expressions can be found in Ref. [14]. The distribution for a modulated Gaussian distribution beam with modulation amplitude a and period k_m is

$$f(r)=\frac{\exp\left(-\frac{r^2}{2\sigma_\mathrm{r}^2}\right)\exp\left(-\frac{z^2}{2\sigma_\mathrm{z}^2}\right)[1+a\cos(k_\mathrm{m}z)]}{(2\pi)^{3/2}\sigma_\mathrm{r}^2\sigma_\mathrm{z}},$$

where σ_r and σ_z are the beam rms transverse and longitudinal size. The form factor is $F=F_\perp F_{//}$, with

$$F_\perp = \exp\left(-\frac{1}{2}k_2\sigma_r^2\sin^2\theta\right),$$

$$F_{//} \approx \exp\left(-\frac{k^2\sigma_\mathrm{z}^2}{2}\right)+\frac{a}{2}\exp\left[-\frac{(k_\mathrm{m}-k)^2\sigma_\mathrm{z}^2}{2}\right].$$

When the bunch size is longer than the emitted wavelength ($k\sigma_\mathrm{z}>1$, $k\sigma_\mathrm{r}>1$), $F\sim0$ and the radiation distribution is linearly proportional to the beam charge distribution. The incoherent OTR has been widely utilized as beam charge monitor [15, 16]. When the bunch duration (or any longitudinal structure inside the bunch) is shorter than the emitted wavelength ($k\sigma_\mathrm{z}<1$, $k\sigma_\mathrm{r}<1$), $F>0$ and the radiated power then scales quadratically with the total charge. The intensity of the coherent emission depends on the value of F. On the other hand, to observe coherent OTR, both transverse and longitudinal charge substructures of a scale at (or below) the optical wavelength are required, thus making it a good candidate for detecting the femtosecond beam structures.

In this work, the measurement of OTR signal based on LPA electrons up to 3.8 meters away from the capillary target is presented. The coherence of the radiation is greatly enhanced with the focusing effect of a pair of quadruples placed right after the capillary exit, demonstrating a femtosecond ultrashort structure inside the bunch.

2 The experiment setup

Figure 1 is the schematic of the experimental setup. The experiment was carried on the LOASIS laser system at LBNL, which delivered 41-fs-duration (Full-Width Half-Maximum intensity) linearly-polarized laser pulses with an on-target energy of 1.3 J. The laser pulse was focused by an off-axis parabolic mirror onto the entrance of a gas filled discharged capillary. The focused beam was measured to have a spot size of r_0=22 μm and a Strehl ratio of 0.7. The corresponding normalized vector potential was $a_0\sim1.2$.

The capillary was laser-machined into 33 mm long sapphire blocks with a diameter around 250 μm. As shown in Fig. 1, pure hydrogen gas was introduced through two gas slots into the capillary and ionized by striking a discharge between electrodes at the capillary ends. A fully ionized channel was formed a few hundred ns after the discharge, with an electron density which increased with radial distance from the axis [17]. The intense laser pulses was guided over a distance several times the Rayleigh range by the preformed plasma channel and the acceleration length was significantly increased. Due to the longer acceleration length, the background plasma density was allowed to decrease from several 10^{19} cm^{-3}, which was standard in a gas jet experiment, to 10^{18} cm^{-3} level, so the acceleration process stayed in a more stable quasi-linear regime and the accelerated electron beam divergence was improved.

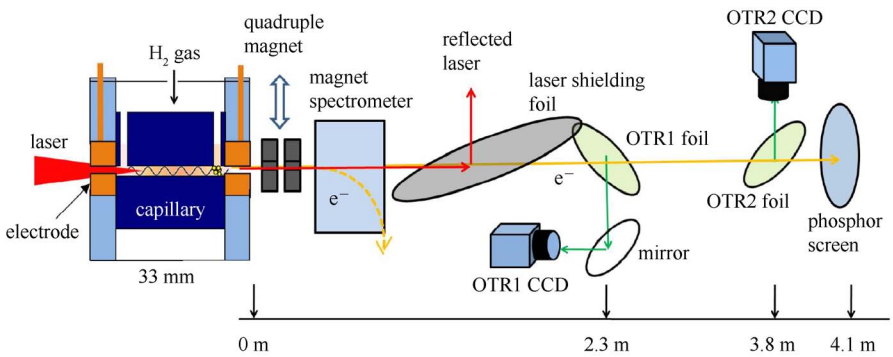

Fig. 1. Schematic of the experimental setup.

Two insertable quadruple magnets were installed right after the capillary [18]. When the magnets were inserted, by scanning their relative positions, the electrons with designed energy were collimated along the propagation axis, while the electrons exceeding the designed energy range were scattered.

A magnetic spectrometer was placed after the quadruple magnets to record the electron energy distribution by deflecting the beam downward onto a phosphor screen [19]. When the magnet was turned off the beam could propagate to the downstream diagnostics. Remnant laser light was deflected and blocked by a 6-micron thick aluminized Mylar foil stacked onto a 14-micron black polycarbonate foil 2 meters away from the target. The foils were placed at an 11-degree angle of laser incidence to reduce the irradiated laser intensity. No visible damage has been observed through the experiments. Coulomb scattering by the foils was negligible due to the relatively high energy (50–500 MeV) in this experiment.

Behind the laser blocking foils, two 5 μm thick aluminum coated Mylar foils were placed 2.3 m (OTR1) and 3.8 m (OTR2) downstream the target, respectively, to generate the OTR signal. They were tilted by 45° angle with respect to the electron axis. Backward OTR signals were simultaneously recorded by two 16 bit pixels CCD cameras. Both cameras were imaging at the surface of each foils, with a calibration of 200 μm spatial resolution and 50 mrad collection angle, which could effectively collect the radiation from electron beam with energy larger than 20 MeV. The observation wavelength range was between 300 nm and 1050 nm set by the CCD spectral response sensitivity. With the extra "Multiplication Gain" feature, the sensitive of OTR2 camera was two orders higher than OTR1 camera. Therefore all the quantitive analyses given in this work were based on the OTR2 measurements to ensure the accuracy. At the end of the beam line, a calibrated phosphor screen was placed to record the beam position and charge distribution.

3 The experiment result

To generate stable and high quality electron beams, the experimental parameters (discharge delay, gas pressure, etc.) were carefully scanned based on the magnetic spectrometer measurements. Fig. 2 shows the variation of electron beam charge (circle) and laser energy transmission (square) as a function of the capillary discharge delay. The capillary injected hydrogen pressure was set at 160 Torr. The inset is the timing plot of the discharge current, where the gray area from 400 ns to 800 ns is the corresponding scanning regime. One can see that the laser energy transmission rate starts to raise after 600 ns of the discharge, indicating the formation of the plasma guiding channel. When the maintained laser field was strong enough, it created plasma wake through which laser energy was deposited into the wake and subsequently to the electrons. As a consequence, the electron beam charge rises following the laser energy transmission and the optimum charge is obtained around 720 ns delay.

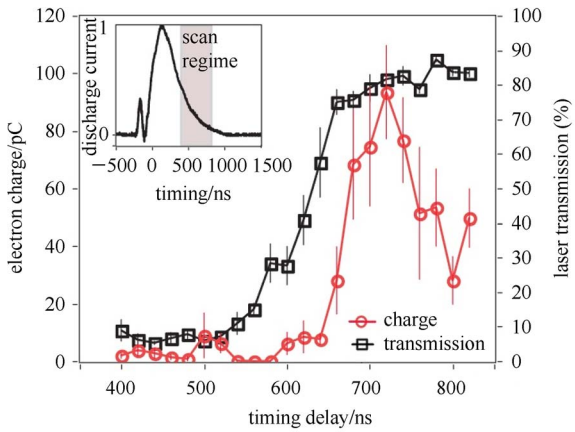

Fig. 2. Electron beam charge (circle) and laser energy transmission (square) as a function of discharge delay, with capillary filling pressure 160 Torr. The large symbols are the averaged value within 20 ns time interval and the error bars show standard deviation. The inset is the timing plot of the discharge current, where the gray area is the corresponding scan regime from 400 ns to 800 ns.

With 160 Torr injected pressure and 720 ns discharge delay set, two quadruple magnets were inserted to further focus the electron beam. Fig. 3 shows the energy spectrum of electron beam measured (a) without and (b) with the quadruple magnets. The broadband energy distribution shown in Fig. 3(a) was possibly caused by the electron continuous injection and rotation in phase space. It could be improved by precisely detuning the laser and plasma parameters, but it was not processed since this experiment was focused on the OTR measurement. As shown in Fig. 3(b), the quadruple magnets worked as a beam selector, collimated and transported the electron beam with energy around 230 MeV. Due to the fact that the OTR stages were behind the energy spectrometer, the measured spectrum was used as an energy reference for the subsequent OTR diagnosis.

When the magnet was turned off, OTR1, OTR2 and the calibrated phosphor screen were used to simultaneously record the OTR near-field images and beam charge profile for every shot. For each OTR image, after subtracting background, it was integrated over the image to get the integrated CCD count number. A parameter called "coherent enhancement" is defined to characterize the coherence level of OTR signal, which is the ratio of the detected OTR signal CCD count number to its

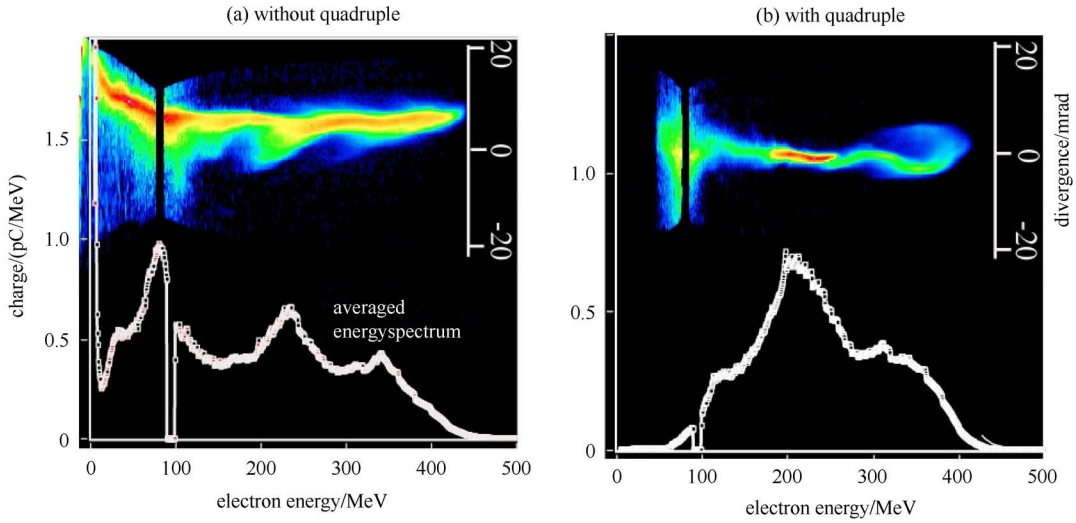

Fig. 3. The electron beam energy spectra measured by the magnet spectrometer, under the conditions of (a) without and (b) with the quadruples focusing.

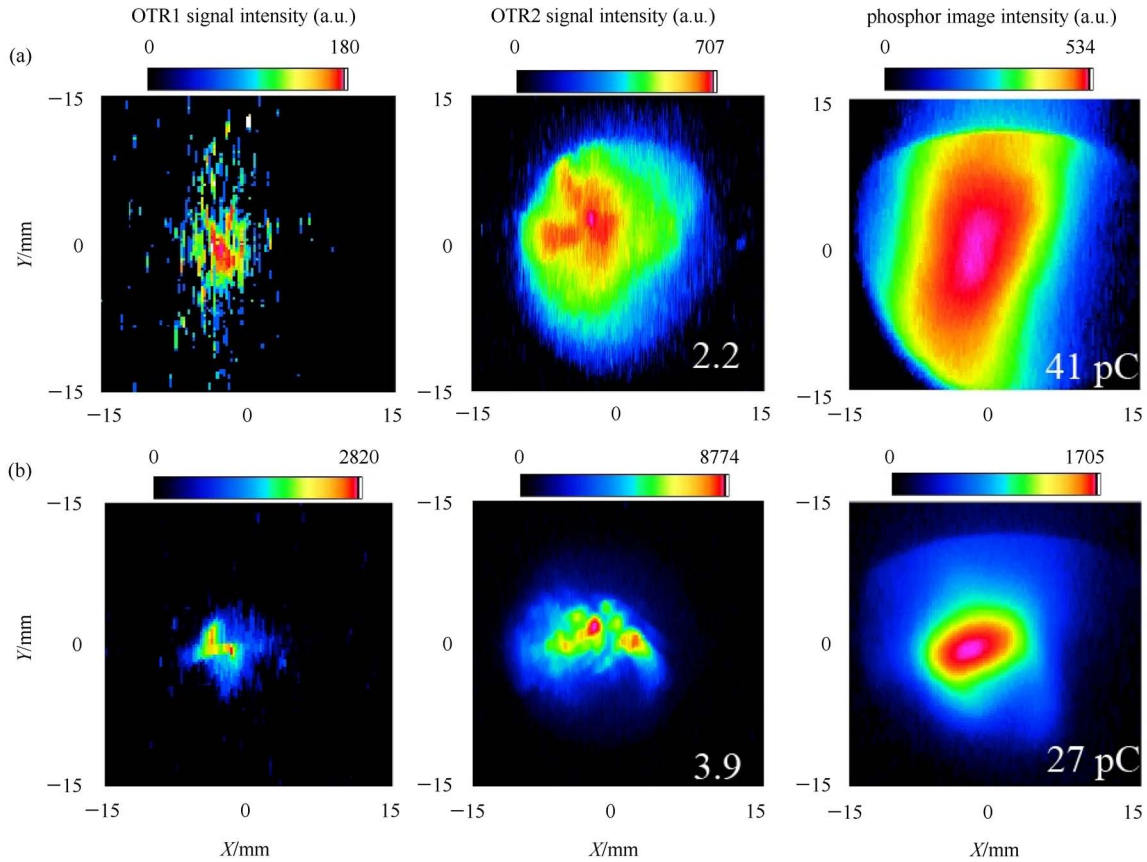

Fig. 4. The simultaneously taken single shot electron OTR1, OTR2 and phosphor near-filed images, under the conditions of (a) without and (b) with the quadruples focusing. In OTR image, the white number is the coherent enhancement calculated based on the whole electron bunch charge. The beam charge information is also shown inside the phosphor image.

estimated incoherent OTR signal CCD count number. The latter one was calculated based on (1) the averaged energy distribution from magnet spectrometer, (2) the beam transverse profile from phosphor screen, (3) the vendor supplied CCD spectral response curve QE and analog-to-digital unit (ADU) conversion efficiency and (4) the imaging system collection efficiency. The radiation is incoherent if the coherent enhancement equals 1. The error level estimated based on the shot to shot beam energy and signal background fluctuation was between 0.7 and 1.8. In order to ensure the accuracy, the radiation was defined as coherent only when its enhancement was larger than 1.8.

Figure 4 shows the single shot electron OTR1 (2.3 m), OTR2 (3.8 m) and phosphor (4.1 m) images, under the condition of (a) without and (b) with the quadruple magnets. The injection pressure and the discharge delay are the same as Fig. 3. The coherent enhancement and beam charge are also marked, respectively, in lower corner of the OTR2 and phosphor images. In Fig. 4 (a), without the focusing magnets, the electron beam divergence is relatively large about 4 mrad (full width at half max). The large beam size suppressed the OTR coherence emission and resulted in a low photon flux. As a consequence, the radiation can barely be detected by the OTR1 CCD. Note that there is an enhanced area distributed at the center of the OTR2 image, which differs from the phosphor image. Considering the low coherent enhancement 2.2 which is only slightly above the error level and the broadband electron beam energy distribution shown in Fig. 3(a), this enhancement can be contributed by both the higher energy electrons and the coherent emission.

When the quadruple magnets were inserted, the transverse beam divergence is reduced to 2.7 mrad (FWHM) with 3 times higher peak charge intensities compared with Fig. 4(a). In contrast, the peak intensities of OTR1 and OTR2 are both increased for more than an order with enhanced intensity well above any fluctuation in electron energy and charge distribution. The OTR images no longer resemble the transverse charge distribution, but exhibit some "hot spikes"- a typical feature for near-field coherent OTR signal [10]. The position of the spots presents the coherent area of the beam, namely, the position of the laser induced microstructure.

4 Conclusions

In conclusion, the OTR detection system has been built and tested on a laser plasma accelerator system. Electrons with energy up to 500 MeV were generated from a cm scale plasma waveguide and characterized by the OTR signal. Coherent OTR, featured with the significant localized spikes in the OTR images, was also observed when the electron beam was focused by two magnetic quadruple lenses. The coherent radiation indicating the existence of ultrashort longitudinal structures inside the electron beam, which may be caused by the direct interaction of the beam and the drive laser.

References

1 Esarey E et al. Rev. Mod. Phys., 2009, **81**: 1229
2 Leemans W et al. Nature Physics, 2007, **2**: 696–699
3 Fuchs M et al. Nature Physics, 2009, **5**: 826–829
4 Ginzburg V et al. Physics Report, 1979, 49
5 Tilborg J et al. Phys. Rev. Lett., 2006, **96**: 014801
6 Debus A et al. Phys. Rev. Lett., 2010, **104**: 084802
7 Lundh O et al. Nature Physics, 2011, **7**: 219–222
8 Glinec Y et al. Phys. Rev. Lett., 2007, **98**: 194801
9 Lumpkin A et al. Phys. Phys. Rev. Lett., 2002, **83**: 234801
10 Loos H et al. Proceeding of FEL08. Gyeongju, Korea, 2008. 485–489
11 Salen P et al. Proceeding of FEL09. Liverpool, UK, 2009. 739–745
12 Lumpkin A et al. Phys. ST. Accel., 2009, **12**: 080702
13 Nemeth K et al. Phys. Rev. Lett., 2008, **100**: 095002
14 Schroeder C et al. Phys. Rev. E, 2004, **69**: 016501
15 Dolgoshein B. Nucl. Instrum. Methods A, 1993, **326**: 434–469
16 Catravas P et al. Proceeding of the 1999 Particle Accelerator Conference. Piscataway, NJ, 1999, **3**: 2111–2113
17 Gonsalves A et al. Phys. Rev. Lett., 2007, **98**: 025002
18 Osterhoff J et al. Proceeding of the 14th Advanced Accelerator Workshop. Annapolis, Maryland. 2010
19 Nakamura K et al. Rev. Sci. Instrum., 2008, **79**: 053301